Spatially Variable Bioturbation and Physical Mixing Drive the Sedimentary Biogeochemical Seascape in the Louisiana Continental Shelf Hypoxic Zone

Richard Devereux[1*], John C. Lehrter[1,2‡], Giancarlo Cicchetti[3], David L. Beddick Jr.[1], Diane F. Yates[1], Brandon M. Jarvis[1], Jessica Aukamp[1], Marilynn D. Hoglund[1]

[1]United States Environmental Protection Agency
National Health and Environmental Effects Research Laboratory
Gulf Ecology Division, 1 Sabine Island Drive, Gulf Breeze FL 32561

[2]University of South Alabama, Department of Marine Sciences, 101 Bienville Blvd, Dauphin Island, AL 36528

[3]United States Environmental Protection Agency
National Health and Environmental Effects Research Laboratory
Atlantic Ecology Division, 27 Tarzwell Drive, Narragansett RI 02882

Running title: Sediment fauna and biogeochemistry

*Corresponding Author: phone 850-934-9346; email devereux.richard@epa.gov

[‡]Present Address: Department of Marine Sciences, University of South Alabama, Dauphin Island Sea lab, 101 Bienville Blvd., Dauphin Island AL 36528

Abstract

Seasonal hypoxia on the Louisiana continental shelf (LCS) has grown to over 22,000 km^2 with limited information available on how low oxygen effects the benthos. Benthic macrofaunal colonization and sediment biogeochemical parameters were characterized at twelve stations in waters 10 – 50 m deep along four transects spanning 320 km across the LCS hypoxic zone in the early fall of 2010 when bottom waters typically return to oxic conditions. Chemical data and sediment profile imaging (SPI) support three primary mechanistic pathways of organic matter degradation on the LCS: (i) metal oxide cycling in depositional muds, (ii) infauna-driven bioturbation delivering oxygen below the sediment-water interface, and (iii) sulfate reduction in sediments where iron oxide availability is limited. The transect nearest the Mississippi River delta had the highest concentrations of porewater and solid phase Mn and Fe with SPI images of recently deposited reddish, mixed muddy sediments suggestive of metal cycling. The deepest stations had high oxidized iron concentrations and rust colored sediments with faunal colonization that suggests sediments are oxidized via bioturbation. Many nearshore and central LCS stations had more black sediments, more disturbed clay layers, lower amounts of oxidized iron, and higher sulfate reduction rates than the deepest stations. Sediment mixing coefficients, D_B, determined from chlorophyll-*a* concentration profiles varied between 33 and 183 cm^{-2} y^{-1}. D_B values were highest at the deepest stations where sediments were colonized. D_B were not determined at two nearshore stations where chlorophyll-*a* concentrations were highly variable in surficial sediments, and on the eastern shelf where sedimentation is high. This study provides a regional view of benthic faunal colonization and sediment biogeochemistry on the LCS, describes regions with potentially different pathways of organic matter degradation, and demonstrates the importance of both bioturbation and physical mixing in processing the large amounts of organic matter in river-dominated continental shelf systems.

Introduction

The Gulf of Mexico Louisiana continental shelf (LCS) is a dynamic region that receives flows from the Mississippi and Atchafalaya rivers. Riverine delivery of nutrients onto the LCS stimulates the production of phytoplankton, and the decay of phytoplankton biomass beneath the pycnocline consumes dissolved oxygen (DO) leading to seasonal (late spring to early fall) bottom-water hypoxia (DO $\leq$ 2.0 mg L^{-1}) that can cover over 22,000 km^2 (Rabalais et al. 2002; NOAA 2017). The presence of hypoxic bottom water can be localized and transient over the course of the LCS hypoxia season (Rabalais et al. 2002). Nonetheless, coastal water hypoxia and high rates of organic matter (OM) deposition can lower sediment redox potential, increase burial and preservation of OM (Hedges and Keil 1995; Middelburg and Levin 2009), alter sediment-water fluxes of carbon, oxygen, and nutrients (Lehrter et al 2012), and impair benthic infauna during prolonged events (Baustian and Rabalais 2009).

The seafloor near the outfall of large rivers such as the Mississippi and Amazon are characteristically meter-thick mobile muds wherein iron oxide reduction dominates OM mineralization because the metal oxides are regenerated as the muds mix with oxygenated water (Aller and Blair 2006; McKee et al. 2004). Sediment deposition and mixing intensities vary across the LCS, which could influence spatial variation in biogeochemical processes. Most of the sediments (90%) settle within the first 10 km and 50 km of the Atchafalaya and Mississippi rivers, respectively (Xu et al 2011). The remainder of LCS hypoxic zone sediments are 80% mud, except for sandy shoals located between the 5 m and 10 m isobaths south of Atchafalaya Bay, and receive 5% of the discharged sediment (Xu et al 2011, 2014). LCS sediments can be resuspended by waves formed during winter storms that disrupt hypoxia and other high wind events (Bianchi et al. 2010). Along the nearshore, waves have sufficient energy to resuspend fine sediments sorting and transporting them across the shelf (Bianchi et al. 2002; Xu et al. 2014). Relic sediments found inshore along the 10 m isobath in the central LCS are well mixed with little near-term sediment accumulation (Allison et al. 2000). On the middle and outer shelf, waves are sufficiently energetic 10% of the time to suspend the upper few mm of fine surficial sediments (Xu et al. 2014). Hurricanes and tropical storms further impact LCS sediment distribution. A single storm can erode up to 8 cm of sediment in waters less than 25 m deep, and 2 cm of sediment in 40 m deep water, transporting and depositing negligible to 15 cm storm layers nearly equivalent to the mass delivered onto the shelf by the rivers in one year (Allison et al. 2010; Goñi et al 2006). In addition, the shelf is an important fishery area where sediments may be disrupted by bottom trawling (LDWF 2018).

Metal cycling may dominate sedimentary OM mineralization in coastal depositional zones (Aller 1998; Beckler et al 2016). Recent LCS sediment studies demonstrated iron and sulfide oxidation in surficial sediments (Reese 2012) with metal oxide reduction accounting for 42-72% of OM mineralization at some locations (Devereux et al. 2015). Mn and Fe oxides are thermodynamically preferred electron acceptors over sulfate and also efficiently oxidize or precipitate sulfide (Thamdrup et al. 1994). Therefore, iron and manganese concentrations may not only constrain sulfate reduction rates (SRR) during transient periods of hypoxia, they could also limit sulfide toxicity towards LCS benthic macrofaunal communities and in turn preserve bioturbation-promoted OM remineralization and redox cycling (Aller 1994). LCS hypoxic zone iron and sulfur cycling have been investigated only at a limited number of sites (Devereux et al. 2015; Reese 2012; Morse and Lin 1991). The distribution of benthic fauna and their relation to sediment biogeochemistry on the LCS are largely unknown.

Sediments delivered by large rivers make disproportionate contributions to global ocean processes, i.e., they are responsible for over 80% of global ocean carbon burial (Berner 1982). Given the Mississippi River ranks 7^{th} in the world for sediment discharge (McKee et al. 2004), a broader spatial view of LCS sediment processes may help advance understanding linkages between bioturbation, biogeochemistry, and organic carbon remineralization on continental shelfs influenced by river discharge.

We hypothesized, because deposition rates and physical mixing of sediments vary across the LCS (Xu et al. 2014), that benthic infaunal colonization, bioturbation, and pathways of OM mineralization will also vary. Here we report results from a fall 2010 cruise to twelve stations across the hypoxic region of the LCS where we measured SRR, determined concentrations of porewater and solid phase Mn and Fe, and used a sediment profiling imaging (SPI) camera to assess sediment redox status and macrofaunal communities. Our findings show LCS sediments are dominated by metal cycling near the Mississippi River delta and, on the remainder, transition from nearshore physically mixed sulfidic sediments to oxidized bioturbated sediments offshore.

Materials and methods

Stations and SPI imaging

Twelve LCS stations on four transects, spaced across 320 km and extending from shallow (8 m) to deeper waters (50 m) were sampled during a cruise from September 26 to October 8, 2010 (Fig. 1, Table 1). Temperatures, salinities, and DO concentrations about 1 m above the sediment surface were recorded with a Sea-Bird 911 CTD (Table 1). Tropical storm Bonnie traversed the study area east of the delta with 40 km h^{-1} winds at the end of July 2010 (National Hurricane Center, 2010a) and may have disturbed sediments at some shallow and mid-depth stations.

The physical structure of the sediments, the presence of macrobenthic organisms, and the depth of oxidized sediment at each station were assessed using a SPI camera (Rhoads and Cande 1971; see Germano et al. 2011 for a thorough review;). These cameras cut into unconsolidated substrates and photograph the sediment profile through an acrylic face plate. Unconsolidated sediments appear red, orange, tan, brown, black, blue, or dark-to-medium gray and sediment grains may be visible. Low porosity clay layers may underlie unconsolidated sediments and appear light gray to white in color. The 10.2-megapixel Nikon D80 camera used in this study imaged a 15.2 cm wide x 22.0 cm deep section of the sediment and overlaying water.

The camera was deployed between 3 and 6 times at each of the 12 sampling stations, resulting in a total of 47 camera images. Images were randomized and renamed so the analyst had no information on station location or environmental setting. Images were enhanced following guidelines of Rossner and Yamada (2004) using Adobe Photoshop 7.0. Sediment features (e.g., fauna, burrows, tubes, sediment layers) were identified as in Nilsson and Rosenberg (1997), Rhodes and Germano (1982), and the Coastal and Marine Ecological Classification Standard (CMECS) (FGDC 2012).

SPI metrics

Five metrics were quantified from each image analyzed. First, the apparent Redox Potential Discontinuity (aRPD) is the depth at which oxygenated red, orange, tan, or brown particles (ferric hydroxides; Teal et al. 2009) visually transition to reduced black, blue, or gray sediments. The aRPD shows the depth of fauna dragging or pumping oxygen into the sediment, is well accepted as a measure of the depth of bioturbation and represents the biological component of the sediment mixing depth (Rhoads and Germano 1982; Rosenberg et al. 2001; Teal et al. 2009). aRPD depth and benthic fauna have been shown to correlate with DO concentrations in the overlying water (Cicchetti et al. 2006), oxygen penetration (Diaz and Trefy 2006), decrease in iron(oxy)hydroxides and increase in acid volatile sulfide concentrations (Statham et al. 2017), and as measured by redox probes, where the oxidation-reduction potential (Eh) of the sediment is zero (Grizzle and Penniman 1991; Rosenberg et al 2001; Simone and Grant 2017).

Four indices of benthic community condition and habitat quality were derived from the images. All indices are based on the Pearson-Rosenberg model of faunal succession (Pearson and Rosenberg 1978) which has become a central tenet of marine benthic ecology. The Pearson-Rosenberg model depicts four stages of infaunal community change associated with increasing levels of stress. At low stress levels (Stage 3), large long-lived and well-established benthic fauna create large, deep burrows (> 1 cm width), large tube structures (> 3 mm wide), feeding pits and mounds. Stage 2 communities (at moderate stress levels) consist of smaller opportunistic fauna typically colonizing the first few centimeters of sediment. At higher stress levels, Stage 1 communities are composed of small surface dwelling worms, and at Stage 0 very few multicellular organisms can survive. The first index we applied, the Organism-Sediment Index or OSI (Rhodes and Germano 1982), includes the aRPD depth together with faunal and sediment parameters corresponding to the Pearson-Rosenberg stages and is considered a sensitive index particularly for low quality habitat areas. The second index, Benthic Habitat Quality or BHQ (Nilsson and Rosenberg 2000), includes the aRPD depth with numeric scores for faunal types, sizes, and abundance related to the Pearson-Rosenberg model. Both indices have been used successfully for many years (Germano 2011). We used the two other indices to isolate parameters specific to fauna. The ‘BHQ Fauna’ index subtracts the aRPD component from BHQ, and the The ‘BHQ Fauna’ index subtracts the aRPD component from BHQ, and the Coastal and Marine Ecological Classification Standard (CMECS) Biotic Group Diversity (‘CMECS

Diversity') is based on the number of Biotic Groups as defined by CMECS (FGDC 2012).. Common CMECS Biotic Groups in this study included "Small Tube-Building Fauna" and "Small Surface-Burrowing Fauna". CMECS Diversity is a measure of functional group richness. Worksheets used to determine index scores are provided in the electronic supplementary material (ESM Table 1).

Seven camera deployments did not capture an analyzable sediment surface due to severely disturbed sediments or the camera sinking into soft mud deeper than the 22 cm faceplate view. The aRPD and community indices could not be calculated for those seven images, but physical parameters of the sediments were informative. A caveat of these profile analyses is the low replication at each station (Table 2) in a setting with high within-station variability, particularly at nearshore stations.

Sediment sampling

Sediment cores (10 cm dia., up to 18 cm deep) with overlying water were obtained using an Ocean Instruments (San Diego, CA) multicorer and held loosely capped at room temperature (~27 °C) until processed, usually within an hour. Triplicate, minimally disturbed cores were collected at each station but it was not always possible to obtain porewater samples for every analysis because of low porosity clay layers or compaction. Cores were sliced inside a nitrogen-filled glove bag at 1.0 cm intervals for the top 4.0 cm of sediment and 2.0 cm intervals thereafter to depths of 12 to 18 cm. The sediment fractions were placed into 250 ml centrifuge bottles that were then tightly closed, taken from the glove bag, and centrifuged at 2,500 x g for 10 min at 10 °C. The bottles were returned to the glove bag where porewater supernatant was carefully withdrawn and filtered (0.22 µM) into vials. Sediments left in the bottles were mixed and distributed to vials and tubes for solid phase analyses. Porewater samples were fixed with 10 µL concentrated HCl per ml for iron and manganese determinations. Solid phase samples were frozen at -70 °C and porewater samples were stored at -20 °C for later analyses. Sediment porosities were determined by drying a known volume of sediment to a constant weight in a 65 °C vacuum oven and then dividing that bulk density by a particle density of 2.65 g ml^{-1} (Burdige 2006).

Sulfate reduction rates and chemical analyses

SRR at each station were determined using triplicate 1.0 cm dia. subcores each obtained from a different 10 cm dia. core. The subcores were equilibrated for 1 hr in the dark at the temperature of the overlying water, injected with 0.05 MBq of carrier free $^{35}SO_4^{-2}$ through pre-drilled holes at 1.0 cm intervals, and incubated for an additional 12 h. The sediments were then extruded from the cores, sliced into the same intervals as the 10 cm dia. cores, and fixed in 50 ml centrifuge tubes containing 10 ml of 10% zinc acetate. The tubes were then placed in a -70 °C freezer for the duration of the cruise and subsequently held at -20 °C until further processed. A one-step distillation with boiling chromous acid under nitrogen was then used to release reduced sulfur from the sediment samples as sulfide which was trapped in 2% zinc acetate (Fossing and Jørgensen 1989). SRR were calculated using the ^{35}S counts obtained from the traps and the specific activity of $^{35}SO4^{-2}$ in the porewater (Fossing and Jørgensen 1989). The amount of sulfide precipitated in each trap was measured with the Cline (1969) assay and will be referred to as total reducible sulfur (TRS). TRS includes the acid volatile fraction that is otherwise released with HCl as the first step of the two-step distillation procedure (Fossing and Jørgensen 1989). Amounts of sulfide typically released from LCS sediments by HCl distillation have been small percentages (~1%) of TRS (Devereux unpubl.). TRS concentrations divided by 2 were used as estimates of pyrite iron (py-Fe) (Aller and Blair 2006).

Concentrations of solid, highly reactive reduced iron, $Fe(II)_{HR}$, and highly reactive total iron, $Fe(T)_{HR}$, were determined with ferrozine using 4 h, 0.2 M oxalate extracts of anoxic and air-dried sediments, respectively (Thamdrup and Canfield 1996). Highly reactive oxidized iron, $Fe(III)_{HR}$, was calculated as the difference between $Fe(T)_{HR}$ and $Fe(II)_{HR}$. Total non-pyrite iron, $Fe(T)_{NP}$, concentrations were determined by inductively coupled plasma mass spectrometry (ICP-MS) with extracts obtained by boiling sediments for 1 min with 12 N HCl (Raiswell et al. 1994). The 12 N HCl extracts were also used to measure solid phase Mn [$Mn_{(S)}$] by ICP-MS. Sediment organic carbon (OC) and organic nitrogen (ON) contents were determined by combustion analysis with a Carlo-Erba CNS Analyzer on hydrochloric acid-fumed sediments. Porewater DIC and NH_4^+ concentrations were measured by flow injection analysis (Hall and Aller 1992), porewater Fe^{2+} concentrations were determined with ferrozine (Stookey 1970), dissolved total Fe [$FeT_{(aq)}$] concentrations were determined with ferrozine following reduction of the sample with hydroxylamine, and porewater Mn [$Mn_{(aq)}$] concentrations were measured by ICP-MS.

Sediment mixing

Chlorophyll-*a* (Chl-*a*) concentrations (C) in sediment fractions were determined by fluorometry on 10 ml methanol extracts of 0.5 g wet weight sediment (Welschmeyer 1994). The resulting profiles were used to calculate sediment mixing coefficients (D_B) following Sun et al. (1991):

$$C = (C_0 - C_\infty)\exp\left(-x\sqrt{k_d/D_B}\right) + C_\infty$$

Boundary conditions were $C = C_0$ at $x = 0$; $C = C_\infty$ at $x = \infty$. D_B was not determined for stations C02 and F04 where the Chl-*a* concentrations were highly variable over the depth of the cores nor at stations A05 and A07 where sedimentation is high and Chl-*a* concentrations did not approach zero. The Chl-*a* decay rate applied to all stations, $k_d = 7.52\ y^{-1}$, was obtained from Chen et al.

(2005) where phytoplankton pigment decomposition rates were estimated from concentration profiles in ^{210}Pb- and ^{7}Be-dated LCS sediment cores obtained from a station about 10 km west of A05 (Fig. 1). D_B values were estimated using a least squares fit of the model profile to Chl-*a* data for the entire length of the cores. D_B at stations with high apparent mixing rates (C11, F07, F08, H04, and H08) were determined as the value where the rate of change in least squares regression varied by less than 0.1% between models of increasing D_B estimates.

Statistical analyses

One-way analysis of variance (ANOVA) was conducted for each biogeochemical sediment variable based on the values in the upper 10 cm of sediment (ESM Table 3) to assess statistical differences among the 12 stations. Two-way ANOVAs were also conducted for each variable to assess differences by water depth and east-west location on the shelf and whether there were interactions between depth and location. For depth, stations were coded as Near, Middle, and Deep: Near = 8-10 m depth, Middle = 18-31 m depth, Deep = 49-50 m depth. For location, stations were coded as eastern (transects A and C) or western (transects F and H) locations. Prior to ANOVA, variables were log transformed. ANOVA and Bonferroni post-hoc multiple comparison procedures were conducted in Matlab (Mathworks Inc.). The software package Primer 7 (Clark and Gorley 2015) was used for principal component analyses (PCA) with square root-transformed and normalized (Z-score) sediment data. Correlations among SPI metrics and sediment biogeochemical variables were evaluated with the Holm's sequential Bonferroni method (Holm, 1979). The sediment variables were also analyzed by group averaged cluster analysis with SIMPROF to test for significance ($p \leq 0.05$) of clusters (Clarke et al. 2008).

Electronic supplementary information.

Supplementary figures, tables, and additional information related to this study are available through the EPA Environmental Dataset Gateway, DOI: 10.23719/1407675.

Results

Properties of the bottom water

Temperature, salinity, and DO concentrations of the bottom water at each station are provided in Table 1. Nearshore station depths ranged from 8 – 10 m with salinities of 29.3 – 33.2; mid-transect station depths ranged from 18 – 31 m with salinities of 33.6 – 35.5; and offshore stations had depths from 49 – 50 m and salinities of 36.1 – 36.4. The non-overlapping ranges for depth and salinity suggested the stations provided sediment samples from three distinct alongshore bands. Temperatures and bottom water DO concentrations generally had negative trends with depth along transects the exception being transect C where bottom water DO was lowest at the shallowest stations (C02). Bottom waters had low DO levels at stations F08, C02, and F07 (2.0 – 3.2 mg L^{-1}).

Sediment structure

Sediments consisted of high porosity sediments overlying compacted clay deposits. The thickest high porosity layers (≥ 0.80) were at stations A05 and A07 along the eastern transect nearest the Mississippi River delta where they extended the full depths of the 18 cm cores. High porosity sediments at stations C02 and F04 were 4-6 cm deep, whereas the remaining stations had very thin high porosity layers of 1 cm or less.

Typical marine soft sediment layers were seen in the SPI images (Fig. 2): tan, brown, orange, or red oxidized sediment at the surface, black or dark grey reduced sediment below that, and in some cases a base of light grey compacted clay. In general, stations in the shallowest waters had the most blackened sediments (F04, C02, A02) suggesting the presence of reduced iron-sulfide minerals, whereas rust-colored sediments in deeper waters, seen at the deepest two stations on each transect to varying degrees (Fig. 2), indicated a deep aRPD and abundant oxidized iron. Sediment clasts (fragments of disturbed sediment redistributed on the surface that may appear as balls or chunks) were present in at least one image at all 12 stations. Clasts are associated with sediment disturbance from physical energy or certain types of faunal activities (e.g., digging by large crabs) and may also be evidence of sediment transport (Rhoads and Germano 1982). Examples of large clasts are seen on the sediment surface in Fig. 2, image H08.

Inshore images showed consistently shallow aRPD layers (Table 2) and a high degree of sediment variability within and among stations that suggests a patchwork of sediment habitats shaped by oxygen regimes and by differing physical forces (Fig. 2). The greatest physical energy can be inferred at easternmost inshore station A02 and westernmost station H03. Images at A02 showed uneven light gray clay layers near the surface, indicative of physical stripping of overlying softer sediments and disruption of the clay layers themselves (Fig. 2, A02 images). High physical energy at station H03 was evidenced by clays very near the sediment surface in two of the six images from that station (Fig. 2, H03) and by hard, coarse shelly sand substrate at the other four (not shown). Station C02 showed light gray sediments above sulfidic muds instead of below, and core data reported a deep highly porous layer between 4 to 6 cm, both inconsistent with compact clay sediments (Fig. 2). We interpret the gray sediment here as a relict aRPD; where brown, tan, or red sediments associated with an aRPD become hypoxic or anoxic and the colors of oxidized sediments fade into the greys forming a relic aRPD that are common in areas of episodic hypoxia (Rhoads and Germano, 1982). Clay layers were not seen at station F04, where all images had deep layers of soft sulfidic mud, suggesting a more quiescent area with high deposition rates and low physical mixing (Fig. 2).

Mid-depth and offshore stations had unconsolidated sediments, few visible clay layers, and aRPD depths between 3.6 and 12.3 cm (Table 2). The camera sank into soft muds deeper than the 22 cm height of the faceplate in at least one deployment at several of these stations. Within-station sediment structure varied less at the eight mid-depth and offshore stations than was seen nearshore. However, one C06 image (Fig. 2, C06 image 2) showed sediment layers mixed by disturbance of some kind (e.g., physical energy, large mobile fauna) and station C11 also showed some variation in the deep clay layers (not visible in Fig. 2). Station H08 images showed large clasts (Fig. 2, H08) and one image with a severely disturbed mud layer (Fig. 2, H08 image 2) or "puzzle fabric" (Valente et al. 1996) which may be due to bottom trawling known to occur in that area (LDWF 2018).

SPI indices of habitat quality

The macrofaunal communities seen with SPI consisted mainly of small burrowing and tube-building worms (likely polychaetes and amphipods), including surface and subsurface deposit feeders (ESM Table 1). No large fauna of body width > 2 mm as defined in CMECS (FGDC 2012) were seen in any image. One image from C11, however, contained a large water-filled, oxidized void (Fig. 2, C11, red arrow) with a lumen height > 5 mm as evidence of larger fauna (FGDC 2012). Most BHQ scores fell within the range of 8 to 12, characterizing the LCS benthos as successional Stage 2 (Nilsson and Rosenberg 2000), or moderately stressed (Table 2).

The BHQ index, which integrates aRPD and fauna, had strong negative correlations to both DIC and NH_4^+ ($p < .0001$, Holm's Bonferroni test). The aRPD correlated very strongly to water depth ($p < .0001$, Holm's Bonferroni) in part due to offshore sediments with deep aRPD layers where an abundance of small burrowing fauna and deep burrows seen as vertical striations in the images oxidize the sediments (Fig. 2). An overall application of faunal measures in this data set was difficult. Due to the near-absence of large fauna and the nature of the indices, the CMECS and BHQ faunal measures were effectively based on the diversity, but not abundance, of only a few categories of small opportunistic species (ESM Table 1). This led to some surprising results, e.g., relatively high opportunist diversity despite low abundance in clays at H03 and in the surface sediments of sulfidic station F04 (Fig. 2). The faunal measures correlated strongly to each other and not to any other parameter.

Sediment mixing coefficients

Chl-*a* profiles and D_B are shown in Figure 3. The median LCS mixing coefficient was 121 $cm^2\ y^{-1}$ in comparison with LCS bioturbation coefficients between 9.78 – 62.58 $cm^2\ y^{-1}$ reported by Briggs et al (2015) at A06, and Chen et al (2005) near A05. Other reported mixing coefficients include 66.43 and 146 $cm^2\ y^{-1}$ as the highest D_B values reported for Long Island Sound and the southwest Baltic Sea, respectively (Sun et al. 1991; Moyrs et al. 2016), and 33 – 730 $cm^2\ y^{-1}$ in 55 – 170 m deep waters off Cape Hatteras (Green et al. 2002).

Nearshore stations had either comparatively low D_B values (A02 = 33.09 $cm^2\ y^{-1}$; H03 = 68.58 $cm^2\ y^{-1}$) or highly mixed sediments (C02 and F04). D_B were not determined for C02 and F04, because of variable Chl-*a* concentrations in upper core fractions. A02 and H03 D_B values compare favorably with values (0.2 – 39.3 $cm^2\ y^{-1}$) reported by Allison et al. (2000) outside Atchafalaya Bay. Low sediment mixing was present in the central LCS at C06 (40.56 $cm^2\ y^{-1}$). D_B values at H04, H08, F07, and F08 were above the median value consistent with the 7 – 12 cm aRPD depths observed at those stations with SPI.

D_B values were not calculated at stations A05 and A07 where high Chl-*a* concentrations likely persist downcore because of high sedimentation rates (10 cm y^{-1}) in that region (Chen et al. 2005). Changes in the shapes of the A05 and A07 Chl-*a* profiles below the aRPD depths indicate disturbances or variation in Chl-*a* sedimentation rates.

Sediment chemistry and sulfate reduction rates

Sediment biogeochemistry over the LCS can be described using the representative depth profiles from stations A07, C02, C06, and C11 in Figure 4. Profiles for the remaining stations, and averages of chemical concentrations and SRR in the top 10 cm of sediment, are provided in the supplementary material (ESM Fig. 1; ESM Fig. 2; ESM Table 3). Stations along transect A had among the highest average concentrations of OC (1.3 – 1.4 %), $Mn_{(S)}$ (11 – 18 µg g^{-1} dw), $Fe(III)_{HR}$ (127 – 147 µg g^{-1} dw), $Mn_{(aq)}$ (65 – 228 µM) and lowest $Fe(II)_{HR}$:$Fe(T)_{HR}$ ratios (0.3) (ESM Fig. 1A – 1C; ESM Table 3). Sediments at A07 had peak concentrations of $Mn_{(aq)}$ near 1.5 cm below the sediment water interface, followed with peak Fe^{2+} concentrations at 1.5 – 3.5 cm (Fig. 4). DIC concentrations at A07 demonstrated a peak within the top 4 cm and then decreased with depth. $Mn_{(s)}$ and $Fe(T)_{HR}$ concentrations decreased slowly with depth. $Fe(II)_{HR}$ accounted for about one-third or less of the $Fe(T)_{HR}$ and increased with depth in the upper 7 cm of sediment as $Fe(T)_{HR}$ decreased. Sediment %OC increased 50% between the first and second fractions and then gradually decreased with depth to about 0.8% at 17 cm. SRR increased from 6.5 to 15.0 µmoles L^{-1} d^{-1} in the sediment horizon below the Fe^{2+} peak.

Sediments in the nearshore (8-10 m depth) and mid (18-31 m depth) regions of the LCS, represented by C02 and C06 (Fig. 4), had less $Mn_{(S)}$, $Fe(III)_{HR}$ (except A02) and higher SRR and DIC than the stations on transect A (ESM Fig. 1; ESM Fig. 2; ESM Table 4). DIC concentrations in station C02 sediments increased with depth and approached 9.0 mM about 11 cm below the sediment water interface (Fig. 4). C02 had lower porewater Mn and higher Fe^{2+} concentrations than and higher SRR A07. Average $Fe(II)_{HR}$:$Fe(T)_{HR}$ ratios were 0.6, twice as high as observed in A07 sediments. Solid phase iron and %OC demonstrated two peaks within the top 12 cm of sediment suggestive of a sediment deposition event. High SRR and low Fe(III)HR at C02 corresponds clearly with black sediments seen in in Fig 2 (image C02). Sediments at station F04 (ESM Fig. 2) were black with similar porewater Fe^{2+} and Mn concentration profiles (106 and 123 µM, respectively in the top sediment fraction), high average $Mn_{(s)}$ concentrations, and high yet variable SRR (ESM Table 3). This station may represent a depositional area of the Atchafalaya River (Allison et al 2000). Station C06 profiles were similar to those at C02, however, C06 sediments had more porewater Fe^{2+} and more oxidized Fe in the surface layers (Fig 4). SRR were lower at C06 than C02, even though the %OC was much higher, and might represent inhibition by $Fe(III)_{HR}$ (Beckler et al 2016). Profiles for F07 and H04 were similar to those of C02 or C06 (EMS Fig. 2).

Sediment at deep LCS stations (water depths of ~ 50 m) west of the delta had lower Mn concentrations than found on transect A. At C11, peaks in porewater Mn and Fe^{2+} occurred in the top sediment fractions (Fig. 4). $Fe(T)_{HR}$ concentrations and $Fe(II)_{HR}$:$Fe(T)_{HR}$ ratios at C11 were similar those seen at A07 in contrast to lower Fe(T) concentrations and higher $Fe(II)_{HR}$:$Fe(T)_{HR}$ ratios at C02 and C06 (EMS Fig. 3). The %OC in C11 sediments declined sharply over the top four sediment fractions from 0.9 to 0.4%. SRR in surficial sediments were higher at C11 than at A07, lower than at C02, and similar to rates at C06.

Sediment chemistry and location

One-way and two-way ANOVAs were applied to obtain a broad overview of spatial sediment variability (ESM Table 4). In one-way ANOVAs, average $Fe(II)_{HR}$ concentration was the only parameter that did not differ significantly (p = 0.06) by station (ESM Table 4). In two-way ANOVAs there were significant differences by water column depth (ESM Fig. 3). Most notably, shallow station sediments had higher ($p < 0.05$) porewater DIC (4.0 – 7.7 mM), and NH_4^+ (113 – 508 µM) concentrations than middle and deep station sediments (ESM Fig. 1A; ESM Fig. 3; ESM Table 4). There were no significant differences in sediment chemical variables between the two eastern- and two westernmost transects, nor were there any significant interactions between depth and location (ESM Table 4).

Cluster analysis (ESM Fig. 4) and PCA (Fig. 5; Table 3) were performed on sediment data to investigate interrelationships of stations and chemistry. PC1 explained 42.3% of sample variation with more negative coefficients (Table 3) for higher porosity and chemistry associated with oxidized sediments (e.g., higher Mn and $Fe(T)_{NP}$ concentrations; ESM Table 3). Sediments at stations A05 and A07, having oxidized, porous, and muddy sediments with high Mn concentrations and deep aRPD depths, plotted on the left side of the PCA separated from stations with more reduced sediments. Station H03 contained hard sandy sediments as seen by SPI and was separated from all other stations on the right side of the plot. The remaining near- and mid-shore stations were arrayed near vertically in the center of the plot by depth, with the deepest stations having more negative PC2 values. PC2 explained 20.6% of sample variation with positive coefficients for chemistry associated with reduced sediments (e.g, high DIC and $Fe(II)_{HR}$) and with temperature, depth, and aRPD as strong variables. PC3, not plotted in Figure 5, accounted for an additional 12.5% (Table 3).

Discussion

The 12 stations in this study spanned 320 km across the LCS hypoxic zone in waters 8 to 50 m deep. Sediment structure, colonization, and biogeochemical parameters differed greatly on the shelf, including variability within stations. Hypotheses for the LCS have emphasized high OM remineralization rates in areas beneath the river plume as it is transported downcoast (Rowe et al. 2002). We previously hypothesized that spatial patterns in benthic sediment fluxes across the whole of the LCS vary more with depth and proximity to the Louisiana Coastal Current (Lehrter et al. 2012), which is a narrow, nearshore, downcoast current of low salinity plume water that extends from the Mississippi River to Texas and Mexico coastal waters (Cochrane and Kelly 1986; Wiseman et al. 1997). Here we assessed spatial variability in the faunal colonization and biogeochemistry of the sediments.

Sediment Profile Imaging

Sediment imagery combined with biogeochemistry led to greater ecological insight than possible with either method alone and offers a compelling visual link to biogeochemical processes. Images showed that fauna throughout the study area consisted mainly of small opportunistic species as has been reported in prior studies of the LCS (Baustian and Rabalais 2009, Briggs et al. 2015). Apart from one large burrow (Figure 2, Image C11), faunal differences among stations were largely related to the number and depth of small infauna and their burrows, with more and deeper fauna associated with greater aRPD and water column depths; evidence that bioturbation was an important driver of sediment oxidation in mid-depth and deeper areas of the LCS. The aRPD correlated strongly with water depth ($p < .0001$, Holm's Bonferroni), and neither of these correlated significantly with any other parameter (ESM Table 2). This correlation is evident in the images (Fig. 2) and is likely due to both increased faunal activity and bioturbation in more quiescent deeper waters less frequently exposed to hypoxia (Rabalais et al. 2002).

The BHQ index correlated strongly and negatively to DIC and NH_4^+ only, both of which similarly correlated only to BHQ and to each other ($p < .0001$, ESM Table 2). Related factors like aRPD, depth, temperature, and chemistry did not correlate to BHQ. BHQ considers both fauna and the aRPD as an integrative measure of fauna and faunal bioturbation, whereas DIC and NH_4^+ are indicative of microbial activity. The BHQ index correlated strongly and negatively to DIC and NH_4^+ only, both of which similarly correlated only to BHQ and to each other ($p < .0001$, ESM Table 2). Related factors like aRPD, depth, temperature, and chemistry did not correlate to BHQ. BHQ considers both fauna and the aRPD as an integrative measure of fauna and faunal bioturbation, whereas DIC and NH_4^+ are indicative of microbial activity. While microbial activities are very high in bioturbated sediments, infaunal activities promote sediment effluxes of DIC and NH_4^+, decreasing their porewater concentrations, which likely contributes to the correlation (Aller 1998; Kristensen and Blackburn 1987). The strong negative correlation between BHQ and both DIC and NH_4^+ further suggests that certain microbial activities, e.g. sulfate reduction, were associated with conditions unfavorable for fauna

Station A02 is of particular interest for variation in OM decomposition pathways. One image from A02 (Fig. 2, A02) shows an uneven (likely scoured) clay layer under blackened sediments and an overlying oxidized surface layer with indications of bioturbation, but the uppermost part of the oxidized layer shows no surface epifauna, suggestive of freshly deposited oxidized sediments. A second image (Fig. 2, A02 image 2) shows apparently freshly deposited sediment with few infauna and slight blackening directly atop an uneven clay layer. Further, the images suggest that sediment deposition and scouring control faunal colonization and OM processing in the that region of the LCS.

Images showed fauna, bioturbation, and oxidized sediments occurring together predominately in the mid-depth and offshore waters. Fauna-mediated metal redox cycling coupled to OM decomposition will be the dominant terminal electron accepting process in these bioturbated sediments (Aller 1998). Metal oxide cycling will also be prevalent in Mississippi River outflow sediments that are highly mixed and where both deposition (Xu et al. 2011) and infaunal colonization, discussed above, apparently vary temporally. In contrast, the two central inshore stations, F04 and C02, had the largest imaged volume of anoxic black sediment as evidence of sulfate reduction (Fig. 2, ESM Fig. 1A). Black sediments at stations A02 and C06 are also indicative of sulfate reduction. C06 is colonized, however hypoxia is known to affect sediment colonization near that station (Baustian et and Rabalais, 2009) and further increases in sulfate reduction due to LCS hypoxia (Devereux et al 2015) could lead to sulfide toxicity.

The closest comparison study for our SPI work is Briggs et al. 2015. That study used SPI, faunal analysis, X-radiography, and Computed Tomography (CT) imaging in the same region of the LCS as our mid-depth stations during the spring and late summer of 2009. A notable difference between the late summer 2009 and our early fall 2010 findings was the much higher status and activity of fauna and deeper aRPD depths in overlapping study areas in the fall of 2010. Fauna in 2009 were early in the recovery trajectory but were much further along in 2010 despite the far larger hypoxic area in 2010 (20,000 km^2 compared to 8000 km^2 in 2009, Turner et al. 2012). It is plausible that mid-depth fauna fared better in 2010 due to an early disruption of hypoxia by Tropical Storm Bonnie in July (National Hurricane Center 2018a), while there were no named storms on the LCS in 2009 (National Hurricane Center 2018b). Sampling in 2010 also took place two weeks later than it did in 2009. Given the much greater spatial extent of hypoxia in 2010, we suggest the higher faunal activity in that year may have been due to an early break-up of hypoxia and longer time for post-hypoxia recovery.

Sediment biogeochemistry and processing of organic matter

Biogeochemical data further support our hypothesis that infauna colonization, bioturbation, metal oxide availability, and thus pathways for OM processing vary across the shelf. Sediment porewater DIC and NH_4^+ concentrations were higher at the nearshore stations ($p < 0.05$, ESM Fig. 3). SRR, Fe (ESM Fig. 1B), and aRPD also exhibited nearshore to offshore gradients with high SRR at shallow stations and low $Fe(II)_{HR}$:$Fe(T)_{HR}$ ratios and deep aRPD depths offshore. Some variables, however, delineated the zone of high sediment deposition near the Mississippi River delta: OC, $Mn_{(s)}$, $Mn_{(aq)}$, and $Fe(III)_{HR}$, concentrations were high at stations A02, A05, A07 (Fig. 4; ESM Fig. 1). The biogeochemical data are congruent with sediment structures and colonization seen in the images that show different modes of sediment mixing over the LCS with generally strong physical mixing nearshore (particularly at A02 and H03) and bioturbation offshore (Fig. 2). A conceptual model of how these OM degradation processes vary over the LCS is presented in Figure 6.

Aller (1998) differentiated continental shelf sediments based on sediment-overlying water interactions, the oxygen content of the overlying water, bioturbation, and sediment accretion rates in relation to pathways of OM decomposition. Biogeochemical zones related to OM processing on the LCS may be characterized as: i) metal oxide redox cycling in depositional river muds near the delta, ii) metal oxide cycling with bioturbation delivering oxygen as much as 10 cm below the sediment-water interface, mainly at offshore sites, and iii) sulfate reduction in sediments where metal oxides are not efficiently recycled, primarily on the nearshore LCS (Fig. 6). Metal cycling in highly mixed mobile muds and sediments can be the most efficient carbon mineralization process (Aller 1994). Next in efficiency, bioturbation-driven degradation of aged or refractory material can be up to ten times more efficient than anaerobic processes alone

(Kristensen 2000). Finally, sulfate reduction is one of the least favorable pathways of microbial respiration and will dominate in the absence of metal redox cycling (Kristensen 2000).

Depositional sediment metal redox cycling

Metal redox cycling defines the depositional zone near the Mississippi River outfall (Fig 6). This is an area of great interest in understanding how large inputs of terrestrial OC to continental shelf systems are processed and buried (Gordon and Goñi 2004). Sediment deposition near the delta can be > 10 cm y^{-1} and is the main factor contributing to burial of OM (Chen et al 2005). The potential for metal cycling in processing OM is greatest at stations A05 and A07 where unconsolidated mud is the thickest and the concentrations of OC, manganese and oxidized iron are highest (Fig. 4, ESM Fig. 1B). Sediments at these stations consisted of orange to rust colored mixed, fine muds and all SPI images showed clasts as evidence of physical disturbance and sediment transport (Fig. 2).

Physical energy mixes muds and greatly expands manganese and iron cycling horizons but may displace or destroy fauna. Consistent with a mobile surface layer, no tube-builders or epifauna were seen in any of the images from transect A (Fig. 2). Bioturbating organisms were present beneath the depauperate surface layers at A05 and appeared to be more abundant at A07, but few were seen at A02 (e.g., A02 Image 2, Fig. 2). Rapid sedimentation and episodic physical forces appear to be the main mechanism that mix LCS depositional sediments such that anaerobic processes are not fully developed. A rapid sedimentation event, suggested by the polyphasic shapes of Chl-*a* profiles (Fig. 3), may have buried affected organisms at A05 and A07.

$Mn_{(S)}$ concentrations in the top 10 cm of sediment along transect A averaged 6.7 µmol ml^{-1} with $Fe(III)_{HR}$ concentrations up to twelve times higher (ESM Table 3, ESM Fig. 1B). Mn oxide reduction in Amazon River mud belts and in sediments with ≤ 10 µmol ml^{-1} is coupled to the rapid oxidation of sulfide and reduced iron (Aller et al. 2010; Jensen et al. 2003; Thamdrup and Dalsgaard 2000). In contrast, up to 80% of OC oxidation was attributed to Mn reduction in some East Sea locations where sedimentary Mn concentrations are high (up to 200 µmol ml^{-1}) (Hyun et al. 2017). Dissolved Fe^{2+} concentrations at A02, A05 and A07 were low in comparison to the high concentrations of porewater Mn(a) and solid $Fe(III)_{HR}$ (Fig. 4, ESM Figs 2C, 3). Mn(s) concentrations in the upper 2 cm of sediments at A05 and A07 (30 and 32 µmol g^{-1}, respectively or ~ 8 µmol ml^{-1} accounting for porosity) may be sufficient to support OC oxidation by Mn reduction. Although redox cycling reactions in muds and depositional sediments may be complex and include suboxic sulfide and NH_4^+ oxidation (Hulth et al 2005; Aller et al 2010), the low SRR at A05 and A07 and biogeochemical profiles are consistent with an importance of microbial Mn(IV) reduction coupled to OM oxidation in sediments near the delta.

Offshore bioturbation

Evidence of bioturbation driving OM decomposition was strongest at the deepest stations and at mid-depth stations on the two westernmost transects. Bioturbation driving OM degradation is therefore an important process on the LCS, especially in deeper waters (Fig. 6). The sediments had orange striations as indicators of faunal activity, little blackening, and deeper aRPD depths than shallow station sediments (Table 2, Fig 2). Sediments stations where SPI indicated bioturbation had the highest mixing coefficients (Fig. 3), low DIC and NH_4^+ concentrations, low $Fe(II)_{HR}$:$Fe(T)_{HR}$ ratios, and low SRR (Fig 4).

Deep waters contribute to favorable benthic habitats in several ways. Principally, deep water sediments have low OM deposition rates and hence low oxygen demand (Berner, 1982) and, on the LCS, infrequent physical mixing from storms (Chen et al., 2015). Lower water temperatures at the deep stations, compared to the nearshore stations (Table 1), will slow microbial activities including DO utilization and SRR. DO concentrations in waters overlying sediments at the deepest stations were low but appear sufficient to support infaunal respiration and bioturbation that would promote oxidation of carbon, NH_4^+, Fe^{2+} and sulfide. Lower DO levels or increased OM loadings at stations with bioturbated sediments could lead to changes in benthic community behaviors, lower bioturbation rates, and sediments becoming more sulfidic relatively deep into the sediments (Diaz and Rosenberg 1995; Rosenberg et al. 2001).

High mixing rates and the presence of numerous small burrowing worms suggest that bioturbation was responsible for the prevalence of oxidized Fe in offshore sediments. It follows that OC processing in this portion of the shelf was largely due to macrofaunal activities. Oxygen introduced to sediments by bioturbation is consumed in the oxidation of reduced Mn, Fe, and S species, so that OM decomposition would mainly be through reduction of Fe(III) (van de Velde and Meysman 2016). C11 was likely influenced by sediment deposition as Fe and Mn concentrations were high like those at A07 and A05. C11, in comparison to A07 and A05, had abundant epifauna and infauna and may represent a transition from the depositional zone to the deeply bioturbated offshore zone.

Nearshore to offshore sediment gradient

Physical disturbance strongly influences infaunal community abundance, composition, and distribution on continental shelf systems influenced by large rivers (Alongi and Robertson 1995). Storms such as tropical storm Bonnie and strong along shore currents that sweep the sediment surface prevent near term LCS sediment accumulation in shallow waters (Allison et al., 2000; Allison et al. 2010; Xu et al. 2011) as evidenced by the shallow disrupted clay layers observed with SPI (Fig. 2). The lack of sediment accumulation together with physical mixing on the nearshore LCS likely limits sediment accumulation and colonization. In addition, the aRPD depth was near the sediment surface at shallow water stations where high DIC, NH_4^+, and $Fe(II)_{HR}$ concentrations, together with high SRR, contribute to a poor benthic habitat. Any faunal colonization in a nearshore portion of the shelf not subjected to strong scouring may have been lost to hypoxia as seen by Baustian et al (2009). Loss of benthic infauna together with hypoxia will promote the development of sulfidic sediments with high DIC and NH_4^+ concentrations (Middleburg and Levin, 2009). This may have occurred at station F04 where sediments have high porewater and solid phase Mn concentrations (ESM Fig. 2) suggestive of an Atchafalaya River sediment deposition zone (Allison et al 2000).

With exception of the eastern shelf depositional zone, LCS sediments inside the 50 m isobath appear to have a gradient from nearshore mainly physically mixed sediments to offshore bioturbated sediments (Figs. 2,3) suggesting a zone of transition in these processes (Fig. 6). This may be illustrated in the alignment of stations by depth along PC2 in the PCA plot (Fig. 5). Shallow stations F04 and C02, near the top of the plot, had the highest SRR (ESM Table 3), images with the deepest layers of black reduced sediments (Fig. 2), and were highly mixed (Fig. 3). Shallow station A02 and central LCS station C06 are below F04 and C02 in the PCA plot. A02 differs from the other eastern transect stations A05 and A07 in having a shallower aRPD, lower sediment Mn concentrations, black sediments and higher water temperatures that may represent transition from the depositional zone (Table 1; Fig. 2; ESM Table 3). C06 had a shallow aRPD with shallow fauna like C02 and A02, and D_B coefficients below the median, warm water temperatures, and high porewater DIC, NH_4^+ and Fe^{2+} concentrations compared to other mid depth stations (Fig. 4). With the loss of benthic fauna activities due to hypoxia or location-specific factors, e.g. at C06 (Baustian and Rabalais 2009), sediment mixing in the central LCS would decrease, iron cycling would slow, and SRR would increase. The cluster of offshore stations with oxidized sediment, high D_B coefficients, cooler water temperatures, low SRR, and where bioturbation appears to drive OM processing are towards the bottom of the PCA plot and represent an offshore bioturbated zone (Fig. 6). Whereas chemical and biological interactions on the shelf are complex, clear patterns of sediment colonization and biogeochemistry emerge supporting our hypothesis of a spatially variable LCS benthos and consistent with LCS sediment fluxes varying with depth and proximity to the Louisiana Coastal Current (Lehrter et al. 2012).

Conclusions

The combination of methods used in this study provided an effective approach to increase understanding of the LCS benthos. The aRPD, BHQ, and the sediment features visible in the SPI images proved to be valuable in explaining sedimentary processes on the LCS. Being able to discern the sediment layering and other features related to sediment mixing provided context when interpreting the physical, biological, and chemical differences among stations. These very different types of data complemented each other well in our study.

Variability in sedimentary habitat and chemistry indicate that OC decomposition pathways in the LCS hypoxic zone are driven by sediment deposition, the mode and extent of sediment mixing, and the history of bottom water hypoxia. Variation in OM pathways and processing efficiency evidenced from the current study portrays the LCS as a three-dimensional mosaic of OM decaying at different rates, through different pathways, in different zones and sediment layers.

Acknowledgements

We thank Jeanne Scott, Leah Oliver, and Jan Kurtz for their help with processing samples during the cruise, and the officers and crew of the now decommissioned USEPA *OSV Bold* for their excellent seamanship and technical assistance. J.C. Lehrter acknowledges partial support from NSF-OE-1760747. This paper is dedicated to the memories of USEPA scientists Diane F. Yates and George Craven in recognition of their many contributions to research at the Gulf Ecology Division. The excellent comments from three anonymous reviewers are greatly appreciated. The views expressed in this paper are those of the authors and do not necessarily reflect the views or policies of the U.S. Environmental Protection Agency.

References

Aller RC (1994) Bioturbaton and remineralization of sedimentary organic matter: effects of redox oscillation. Chem Geol 114:331-345

Aller RC (1998) Mobile deltaic and continental shelf muds as suboxic, fluidized bed reactors. Mar Chem 61:143-155

Aller RC, Blair,NE (2006) Carbon remineralization in the Amazon–Guianas tropical mobile mudbelt: a sedimentary incinerator. Cont Shelf Res 26:2241–2259

Aller RC, Madrid V, Chistoserdov A, Aller JY, Heilbrun C (2010) Unsteady diagenetic processes and sulfur biogeochemistry in tropical deltaic muds: implications for oceanic isotope cycles and the sedimentary record. Geochim Cosmochim Acta 74:4671-4692

Allison MA, Dellapenna TM, Gordon ES, Mitra S, Petsch ST (2010) Impact of Hurricane Katrina (2005) on shelf organic carbon burial and deltaic evolution. Geophys Res Lett 37:doi:10.1029/2010GL044547

Allison MA, Kineke GC, Gordon ES, Goñi MA (2000) Development and reworking of a seasonal flood deposit on the inner continental shelf off the Atchafalaya River. Cont Shelf Res 20:2267-2294

Alongi DM, Robertson AI (1995) Factors regulating benthic food chains in tropical river deltas and adjacent shelf areas. Geo-Mar Lett 15:145-152

Baustian MM, Rabalais NN (2009) Seasonal composition of benthic macroinfauna exposed to hypoxia in the northern Gulf of Mexico. Estuar Coasts 32:975-983

Beckler JS, Kiriazis N, Rabouille C, Stewart FJ, Taillefert M (2016) Importance of microbial iron reduction in deep sediments of river-dominated continental margins. Mar Chem 178:22-34

Berner RA (1982) Burial of organic carbon and pyrite sulfur in the modern ocean: its geochemical and environmental significance. AmerJ Sci 282:451-473

Bianchi TS, DiMarco SF, Cowan Jr. JH, Hetland RD, Chapman R, Day JW, Allison MA (2010) The science of hypoxia in the northern Gulf of Mexico: a review. Sci Tot Environ 408:1471-1484

Bianchi TS, Mitra S, McKee M (2002) Sources of terrestrially-derived carbon in the lower Mississippi River and Louisiana shelf: implications for differential sedimentation and transport at the coastal margin. Mar Chem 77:211–223

Briggs KB, Hartmann VA, Yeager KM, Shivarudrappa S, Diaz RJ, Ostermann LE, Reed AH, (2015). Influence of hypoxia on biogenic structure in sediments on the Louisiana continental shelf. Estuar Coastal Shelf Sci 164:147-160

Burdige DJ (2006) Geochemistry of Marine Sediments. Princeton University Press, Princeton New Jersey. 609 pp

Chen N, Bianchi TS, McKee BA (2005) Early diagenesis of chloropigment biomarkers in the lower Mississippi River and Louisiana shelf: implications for carbon cycling in a river-dominated margin. Mar Chem 93:159-177

Cicchetti G, Latimer J, Rego S, Nelson W, Bergen B, Coiro L (2006) Relationships between near-bottom dissolved oxygen and sediment profile camera measures. J Mar Sys 62:124-141

Clarke KR, Gorley RN (2015) PRIMER v7: User Manual/Tutorial. PRIMER-E, Plymouth, U.K., 296pp

Clarke KR, Somerfield PJ, Gorley RN (2008) Testing of null hypotheses in exploratory community analyses: similarity profiles and biota-environment linkage. J Exp Mar Biol Ecol 366:56-69

Cline JD (1969) Spectrophotometric determination of hydrogen sulfide in natural waters. Limnol Oeanogr 14:454-458

Cochrane JD, Kelly FJ (1986) Low-frequency circulation on the Texas-Louisiana continental shelf. J Geophys Res 91:10645-10659

Devereux R, Lehrter JC, Beddick Jr DL, Yates DF, Jarvis BM (2015) Manganese, iron, and sulfur cycling in Louisiana continental shelf sediments. Cont. Shelf Res 99:46-56

Diaz RJ, Trefy JH (2006) Comparison of sediment profile image data with profiles of oxygen and Eh from sediment cores. J Mar Sys 62:164-172

Diaz RJ, Rosenberg R (1995) Marine benthic hypoxia: a review of its ecological effects and the behavioural responses of benthic macrofauna. Oceangr Mar Biol Ann Rev 33:245-303

Fossing H, Jørgensen BB (1989) Measurement of bacterial sulfate reduction in sediments: evaluation of a single-step chromium reduction method. Biogeochem 8:205–222

FGDC; Federal Geographic Data Committee (2012) Coastal and Marine Ecological Classification Standard (CMECS) version IV. FGDC-STD-018-2012. Available online at https://iocm.noaa.gov/cmecs/. Accessed 7-12-2017

Germano JD, Rhoads DC, Valente RM, Carey DA, Solan M (2011) The use of sediment profile imaging (SPI) for environmental impact assessments and monitoring studies: lessons learned from the past four decades. Oceanogr Mar Biol 49:235-298

Goñi MA, Gordon ES, Monacci NM, Clinton R, Gisewhite R, Allison MA, Kineke G (2006) The effect of Hurricane Lili on the distribution of organic matter along the inner Louisiana shelf (Gulf of Mexico, USA). Cont Shelf Res 26:2260-2280

Gordon ES, Goñi MA (2004) Controls on the distribution and accumulation of terrigenous organic matter in sediments from the Mississippi and Atchafalaya river margin. Mar Chem 92:331-352

Green MA, Aller RC, Cochran JK, Lee C, Aller JY (2002) Bioturbation in shelf/slope sediments off Cape Hatteras, North Carolina: The use of ^{234}Th, Chl-*a*, and Br^- to evaluate rates of particle and solute transport. Deep Sea Res II 494627-4611

Grizzle RE, Penniman CA (1991) Effects of organic enrichment on estuarine macrofaunal benthos: a comparison of sediment profile imaging and traditional methods. Mar Ecol Progr Ser 74:249-262

Hall POJ, Aller RC (1992) Rapid, small-volume flow injection analysis for ΣCO_2 and NH_4^+ in marine and fresh waters. Limnol Oceaogr 37:1113–1119

Hedges JI, Keil R (1995) Sedimentary organic matter preservation; an assessment and speculative synthesis. Mar Chem 49: 81–115

Holm S (1979) A simple sequentially rejective multiple test procedure. Scand J Stat 6: 65–70.

Hulth S, Aller RC, Canfield DE, Dalsgaard T, Engström P, Gilbert F, Sundbäck, Thamdrup B (2005) Nitrogen removal in marine environments: recent findings and future research challenges. Mar Chem 94:125-145

Hyun J-H, Kim S-H, Mok J-S, Cho H., Lee T, Vandieken V, Thamdrup B (2017) Manganese and iron reduction dominate organic carbon oxidation in surface sediments of the deep Ulleung Basin, East Sea. Biogeosci 14:941-958

Jensen MM, Thamdrup B, Rysgaard S, Holmer M, Fossing H (2003) Rates and regulation of microbial iron reduction in sediments of the Baltic-North Sea transition. Biogeochem 65:295-317

Kristensen E (2000) Organic matter diagenesis at the oxic/anoxic interface in coastal marine sediments, with emphasis on the role of burrowing animals. Hydrobiol 426:1–24

Kristensen E, Blackburn TH (1987) The fate of organic carbon and nitrogen in experimental marine sediment systems: influence of bioturbation and anoxia. J Mar Res 45:231-257

Lehrter JC, Beddick Jr DL, Devereux R, Yates DF, Murrell MC (2012) Sediment-water fluxes of dissolved inorganic carbon, O_2, nutrients, and N_2 from the hypoxic region of the Louisiana continental shelf. Biogeochem 109-233-252

LDWF; Louisiana Department of Wildlife and Fisheries (2018) Shrimp Season http://wlf.louisiana.gov/fishing/shrimp-seasons Acccessed 7 December 2018

McKee BA, Aller RC, Allison MA, Bianchi TS, Kineke GC (2004) Transport and transformation of dissolved and particulate materials on continental margins influenced by major rivers: benthic boundary layer and seabed processes. Cont Shelf Res 24:899–926

Middelburg JJ, Levin LA (2009) Coastal hypoxia and sediment biogeochemistry. Biogeosci 6:1273–1293

Morse JW, Lin S (1991) Sulfate reduction and iron sulfide mineral formation in Gulf of Mexico anoxic sediments. Am J Sci 291:55-89

Morys C, Forster S, Graf G (2016) Variability of bioturbation in various sediment types and on different spatial scales in the southwestern Baltic Sea. Mar Ecol Prog Ser 557:31-49

National Hurricane Center (2018a) 2010 Atlantic hurricane season. https://www.nhc.noaa.gov/data/tcr/AL032010_Bonnie.pdf Accessed 14 December 2018

National Hurricane Center (2018b) 2009 Atlantic hurricane season. https://www.nhc.noaa.gov/data/tcr/index.php?season=2009&basin=atl Accessed 14 December2018

Nilsson HC, Rosenberg R (1997) Benthic habitat quality assessment of an oxygen-stressed fjord by surface and sediment profile images. J Mar Sys 11:249-264

Nilsson HC, Rosenberg R (2000) Succession in marine benthic habitats and fauna in response to oxygen deficiency: analysed by sediment profile imaging and by grab samples. Mar Ecol Progr Ser 197:139-149

NOAA (2017) Gulf of Mexico ‘dead zone’ is the largest ever measured. National Oceanic and Atmospheric Administration. http://www.noaa.gov/media-release/gulf-of-mexico-dead-zone-is-largest-ever-measured. Accessed 16 April 2018

Pearson TH, Rosenberg R (1978) Macrobenthic succession in relation to organic enrichment and pollution of the marine environment. Oceanogr Mar Biol 16:229-311

Rabalais NN, Turner RE, Wiseman Jr WJ (2002) Gulf of Mexico hypoxia, A.K.A. “The Dead Zone”. Ann Rev Ecol Syst 33:235–263

Raiswell R, Canfield DE, Berner RA (1994) A comparison of iron extraction methods for the determination of degree of pyritisation and the recognition of iron-limited pyrite formation. Chem Geol 111:101-110

Reese BK, Mills HJ, Dowd SE, Morse JW (2012) Linking molecular microbial ecology to geochemistry on a coastal hypoxic zone. Geomicrobiol J 302:160–172

Rhoads DC, Cande S (1971) Sediment profile camera for in situ study of organism-sediment relations. Limnol Oceanogr 16:110-114

Rhoads DC, Germano JD (1982) Characterization of organism–sediment relationships using sediment profile imaging: An efficient method of Remote Ecological Monitoring of the Seafloor (REMOTS® System). Mar Ecol Progr Ser 8:115–128

Rossner M, Yamada KM (2004) What’s in a picture? The temptation of image manipulation. J Cell Biol 166:11-15

Rosenberg R, Nilsson HC, Diaz RJ (2001) Response of benthic fauna and changing sediment redox profiles over a hypoxic gradient. Estuar Coast Shelf Sci 53:343-350

Rowe GT, Cruz Kaegi MA, Morse JW, Boland GS, Escobar Briones EG (2002) Sediment community metabolism associated with continental shelf hypoxia, northern Gulf of Mexico. Estuar 25:1097-1106

Simone M, Grant J (2017) Visual assessment of redoxcline compared to electron potential in coastal marine sediments. Estuar Coast Shelf Sci 188:156-162

Statham PJ, Homoky, Parker ER, Klar JK, Silburn B, Poulton SW, Kröger S, Pearce RB, Harris EL (2017) Extending the applications of sediment profile imaging to geochemical interpretations using colour. Cont Shelf Res doi.org/10.1016/j.csr.2017.12.001

Stookey LL (1970) Ferrozine—a new spectrophotometric reagent for iron. Anal Chem 42:779–781

Sun M, Aller RC, Lee C (1991) Early diagenesis of chlorophyll-a in Long Island Sound sediments: a measure of carbon flux and particle reworking. J Mar Res 49:379-401

Teal LR, Parker R, Fones G, Solana M (2009) Simultaneous determination of in situ vertical transitions of color, pore-water metals, and visualization of infaunal activity in marine sediments. Limnol Oceanogr 54:1801-1810.

Thamdrup B, Canfield DE (1996) Pathways of carbon oxidation in continental margin sediments off central Chile. Limnol Oceanogr 41:1629–1650

Thamdrup B, Dalsgaard T (2000) The fate of ammonium in anoxic manganese oxide-rich marine sediment. Geochim. Cosmochim. Acta 64, 4157-4164

Thamdrup B, Fossing H, Jørgensen B (1994) Manganese, iron, and sulfur cycling in a coastal marine sediment, Aarhus Bay, Denmark. Geochim. Cosmochim. Acta 58, 5115-5129

Turner RE, Rabalais NN, Justic D (2012) Predicting summer hypoxia in the northern Gulf of Mexico: redux. Mar Poll Bull 64:319-324

Valente RM., Evans NC, Whiteside PGD (1996) Environmental monitoring in Hong Kong using the REMOTS seabed camera. Coastal Management in Tropical Asia: A Newsletter for Practitioners 6:26-29

van de Velde S, Meysman FJR (2016) The influence of bioturbation on iron and Sulphur cycling in marine sediments: a model analysis. Aquat Geochem 22:469-504

Welschmeyer NA (1994) Fluorometric analysis of chlorophyll *a* in the presence of chlorophyll *b* and pheopigments. Limnol Oceanogr 39:1985-1992

Wiseman WJ, Rabablais NN, Turner RE, Dinnel SP, Mac-Naughton A (1997) Seasonal and interannual variability within the Louisiana coastal current: stratification and hypoxia. J Mar Syst 12:237-248

Xu K, Corbett DR, Walsh JP, Young D, Briggs KB, Cartwright GM, Friedrichs CT, Harris CK, Mickey RC, Mitra S (2014) Seabed erodibility variations on the Louisiana continental shelf before and after the 2011 Mississippi River flood. Estuar Coast Shelf Sci 149:283-293

Xu K, Harris CK, Hetland RD, Kaihatu JM (2011) Dispersal of Mississippi and Atchafalaya sediment on the Texas—Louisiana shelf: model estimates for the Year 1993. Cont Shelf Res 31:1558–1575

Figure Captions.

Figure 1

Study area on the Louisiana continental shelf. Stations are identified by filled circles, water column depths (m) are indicated by the dashed contour lines.

Figure 2

Sediment profile images. Left four columns show representative images for each station; right column shows variation at specific stations. Images were cropped to show approximately 10 cm of sediment depth, corresponding to the 10 cm depths over which cores were averaged in analysis of biogeochemical variables. Scale bars at left of each image are 2 mm wide and show 1 cm increments. The red, brown, tan, rust, or orange sediments are oxidized aRPD layers, dark black sediments are evidence of sulfate reduction, and light grey layers are either clays or relic aRPDs. Arrows are used to illustrate select features in images: red arrows indicate water-filled burrows or feeding voids as black scar-like features; white arrows show the protrusions of surface tube-building fauna; the yellow arrow is a worm transected by the camera prism; green arrows point to worm burrows visible as vertical striations of oxidized sediment; and black arrows show sediment clasts. All images have been enhanced to better reveal sedimentary features.

Figure 3.

Chlorophyll-a concentrations in sediment core fractions. The plots are of triplicate cores from each station. Dashed lines indicate the aRPD depth determined from SPI images. D_B values (cm^2 y^{-1}) calculated from Chl-a profiles at each station are provided at the lower right of the plots.

Figure 4.

Profiles of sediment chemistry and sulfate reduction rates. Profiles of sediment porewater $Mn_{(aq)}$, Fe^{2+}, and DIC concentrations (left column); solid phase Mn(s), $Fe(II)_{HR}$, and $Fe(III)_{HR}$ concentrations (center column), and sediment % organic carbon and SRR (right column). Stations represented are (top to bottom rows) A07, C02, C06 and C11.

Figure 5.

PCA of sediment physical/chemical variables at the LCS stations. Stations within the ellipses formed groups by group average clustering of Euclidean distances and SIMPROF analysis at the 5% significance level.

Figure 6.

Zones of OM decomposition pathways on the LCS. The nearshore Physically Mixed – Sulfidic zone (gray) has low faunal colonization and evidence from SPI images of physical disturbances and scouring with the highest rates of sulfate reduction. This zone is highly variable between

A02, having scoured sandy sediments, and H03 where scoured sediments contain shell hash. The central portion of the nearshore zone at F04 has a deeper sandy surface layer with evidence of mixing from Chl-*a* profiles. Sediments in the central nearshore may be colonized when waters are not hypoxic. The Transitional zone (green) along the mid-depth shelf generally has more infaunal colonization, lower sulfate reduction rates, and more oxidized Fe than the Physically Mixed zone. Bioturbation is an important process in this zone but the infauna may be susceptible hypoxia and the sediments may become sulfidic. The Bioturbated zone (orange) is the most colonized zone on the shelf and Fe cycling will be important in OM decomposition. Sulfate reduction is this zone is low and the infauna are less susceptible to hypoxia than in the Transitional zone. The Depositional zone (tan) is the region of high sediment deposition rates, has temporally variable sediment colonization and much more Mn and Fe than any other zone, and Mn cycling may be important in OM processing.

Figure 1

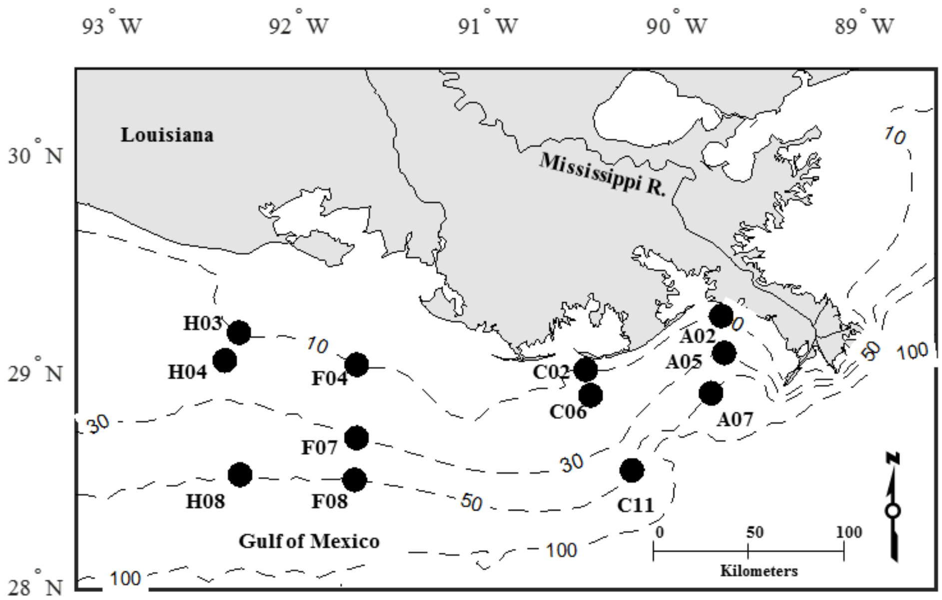

93° W
92° W
91° W
90° W
89° W
30° N
29° N
28° N
Louisiana
Mississippi R.
Gulf of Mexico
H03
H04
F04
C02
C06
A02
A05
A07
F07
H08
F08
C11
10
30
50
100
0
50
100
Kilometers
N

Figure 2

Click here to access/download;Figure;Fig2 12_20_2018.jpg

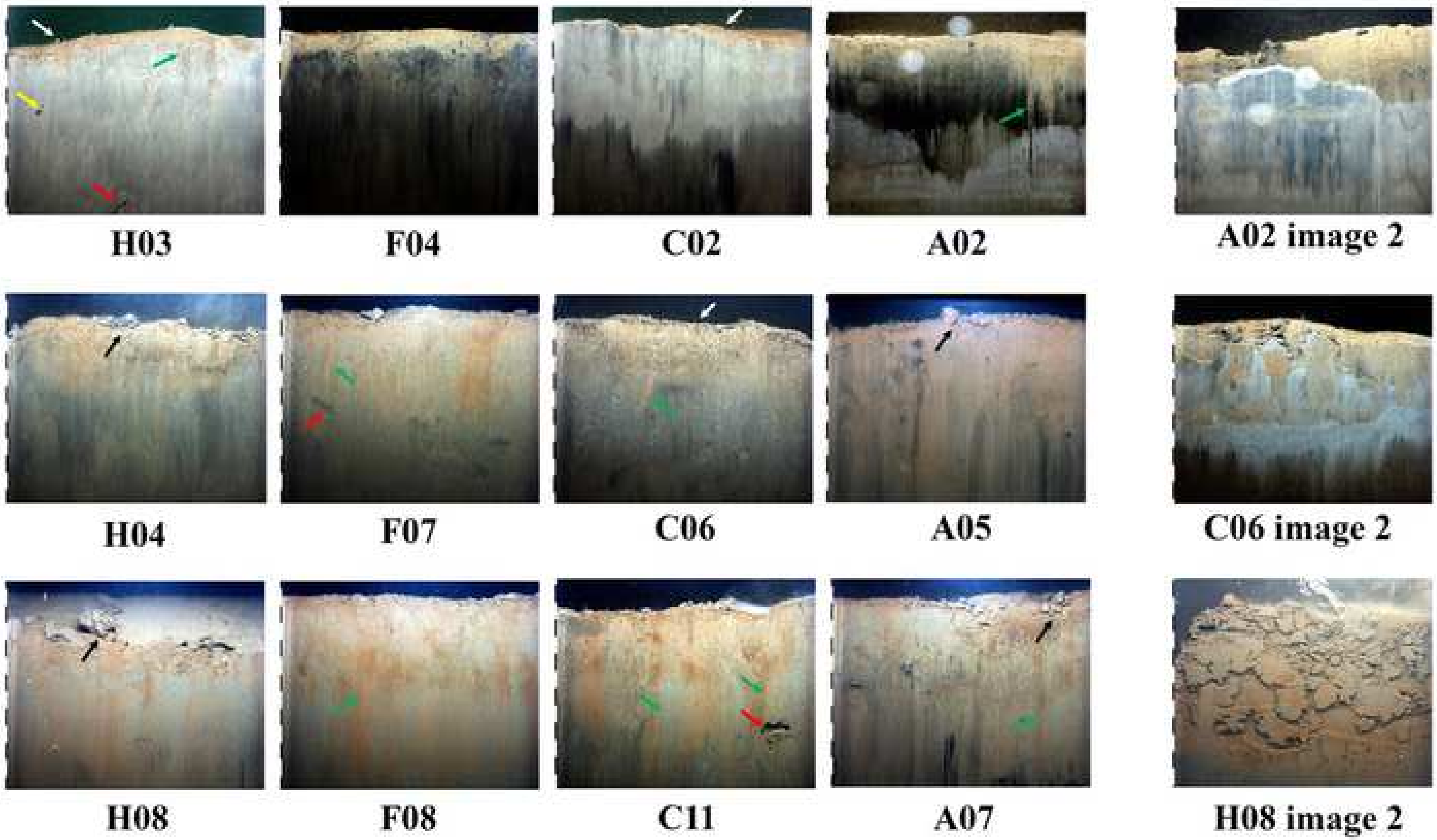

Figure 3

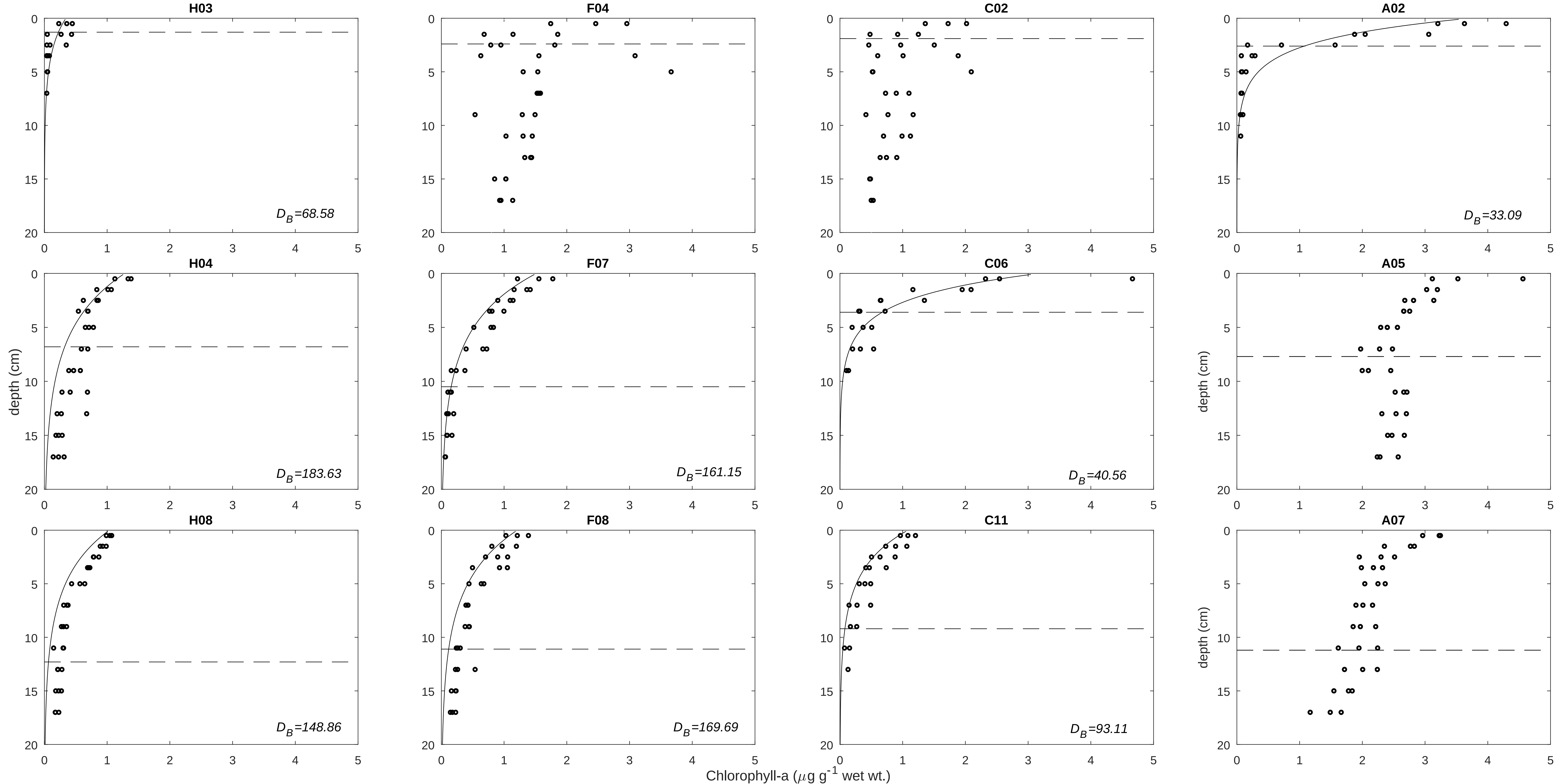

H03
F04
C02
A02
H04
F07
C06
A05
H08
F08
C11
A07
D_B=68.58
D_B=33.09
D_B=183.63
D_B=161.15
D_B=40.56
D_B=148.86
D_B=169.69
D_B=93.11
depth (cm)
Chlorophyll-a (μg g^{-1} wet wt.)

Figure 4

Click here to access/download;Figure;Fig 4 color.jpg

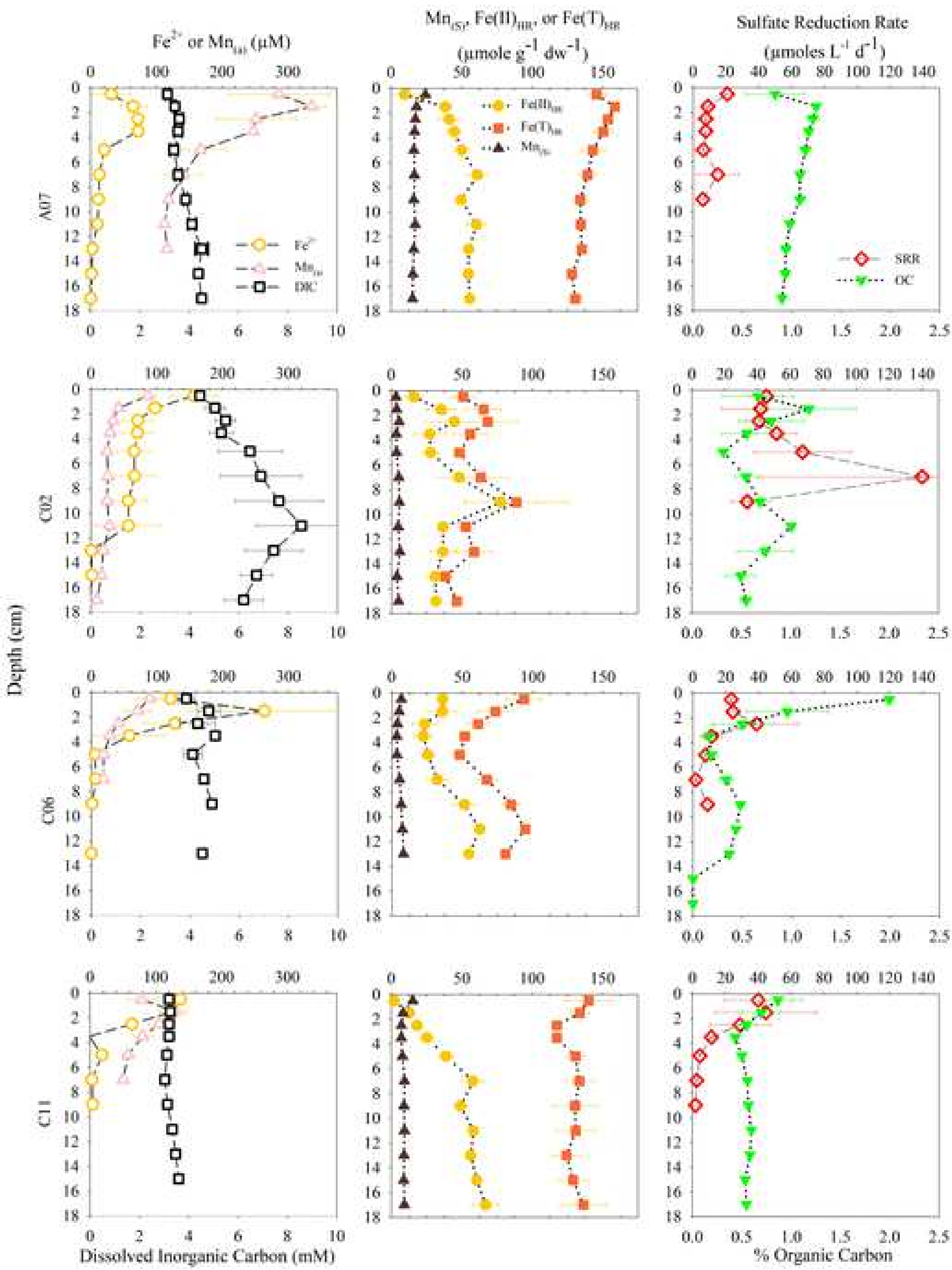

Figure 5

Click here to access/download;Figure;Color Figure 5 PCA.jpg

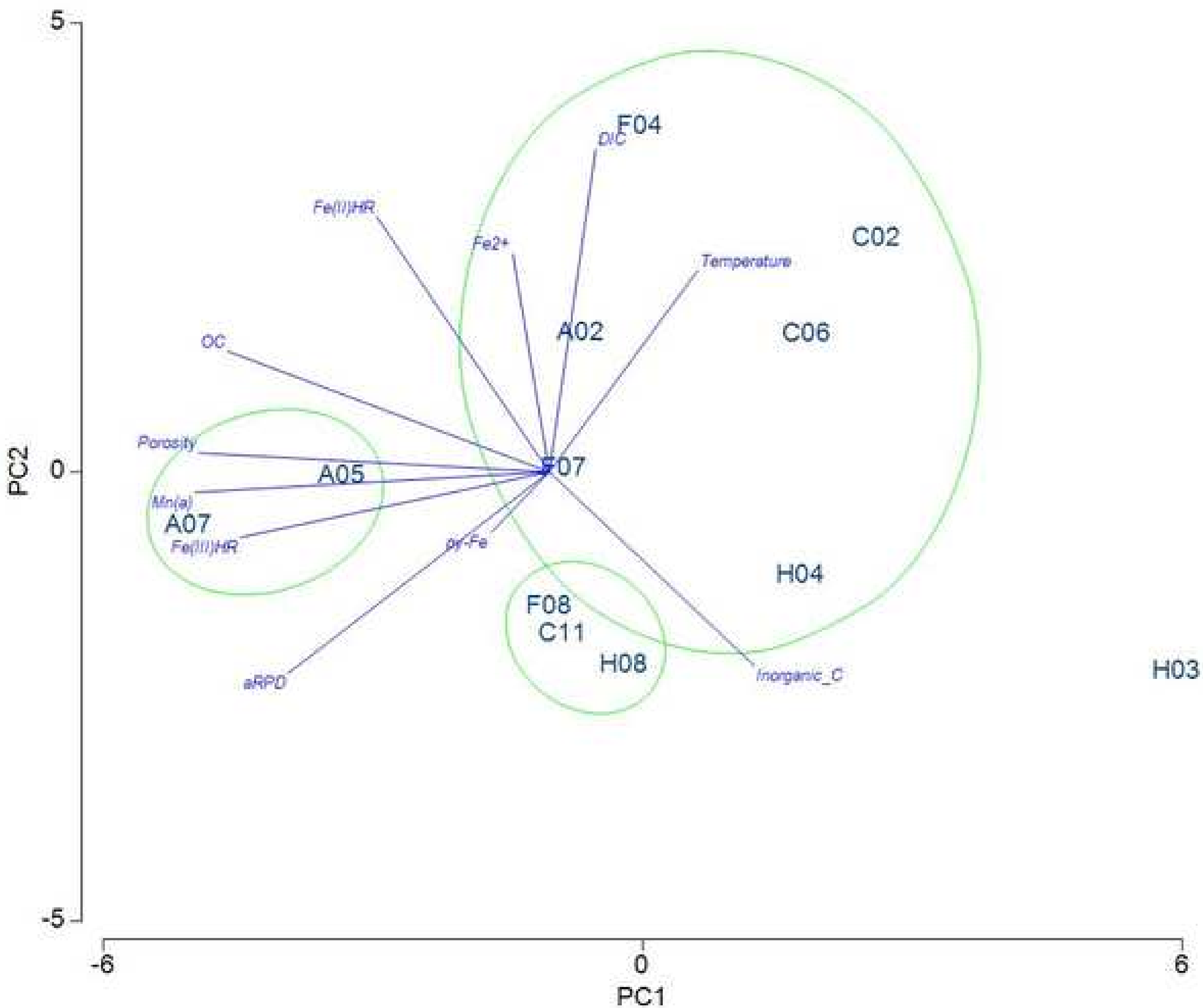

Figure 6

Click here to access/download;Figure;Fig 6 ConceptualMap.tif

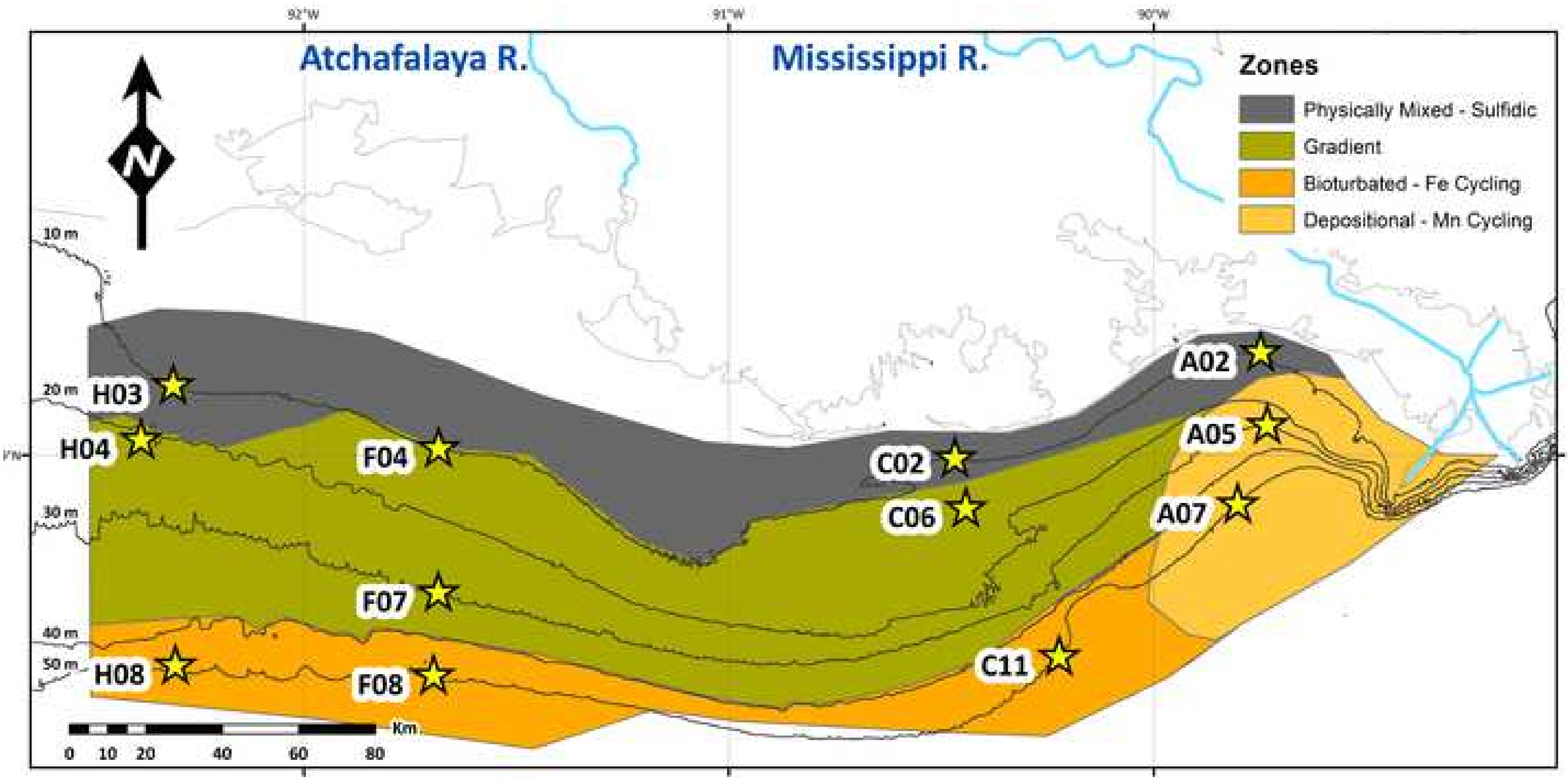

Table 1. Station locations and bottom water hydrography.

Station	Sampling Date	Latitude	Longitude	Water depth (m)	Temperature (°C)	Salinity (PSU)	DO (mg l^{-1})
A02	26-Sep-2010	29.241	-89.749	9	29.1	31.1	6.3
A05	27-Sep-2010	29.070	-89.733	29	27.7	35.5	4.4
A07	28-Sep-2010	28.884	-89.803	49	23.3	36.2	3.9
C02	1-Oct-2010	28.992	-90.468	10	29.2	33.2	2.3
C06	30-Sep-2010	28.874	-90.442	18	29.1	34.2	4.3
C11	29-Sep-2010	28.526	-90.223	50	21.0	36.4	4.5
F04	6-Oct-2010	29.015	-91.683	10	25.2	29.8	7.1
F07	7-Oct-2010	28.676	-91.684	31	26.3	35.4	3.2
F08	8-Oct-2010	28.481	-91.695	50	23.1	36.1	2.0
H03	3-Oct-2010	29.163	-92.308	8	26.8	29.3	6.0
H04	4-Oct-2010	29.035	-92.384	21	28.1	33.6	5.5
H08	5-Oct-2010	28.505	-92.303	50	22.2	36.2	3.8

Table 2. aRPD depths (cm) and sediment habitat quality index values obtained by the analysis of images obtained with the sediment profile imaging camera. *n*, number of images used; *S.D.*, standard deviation.

Station	**aRPD**	*n*	*S.D.*	**OSI**	*n*	*S.D.*	**BHQ**	*n*	*S.D.*	**BHQ Fauna**	*n*	*S.D.*	**CMECS Diversity**	*n*	*S.D.*
A02	**2.6**	2	0.1	**5.0**	2	0.0	**6.5**	2	0.7	**3.5**	2	0.7	**2.0**	2	0.0
A05	**7.7**	2	1.1	**9.0**	2	0.0	**10.0**	2	0.0	**5.0**	2	0.0	**3.0**	2	0.0
A07	**11.2**	2	1.9	**9.0**	2	0.0	**11.5**	2	2.1	**6.5**	2	2.1	**3.5**	2	0.7
C02	**1.9**	3	1.6	**5.3**	3	3.1	**8.7**	3	2.3	**6.3**	3	1.2	**3.3**	3	1.2
C06	**3.6**	3	0.3	**8.3**	3	0.6	**10.7**	3	0.6	**7.3**	3	0.6	**4.3**	3	0.6
C11	**9.2**	4	1.5	**9.5**	4	1.0	**13.5**	4	1.0	**8.5**	4	1.0	**4.8**	4	0.5
F04	**2.4**	3	1.0	**6.0**	3	1.0	**9.0**	3	1.0	**6.3**	3	1.2	**3.3**	3	1.2
F07	**10.5**	2	1.0	**8.0**	2	1.4	**11.0**	2	1.4	**6.0**	2	1.4	**3.0**	2	1.4
F08	**11.1**	2	0.5	**7.0**	2	0.0	**10.5**	2	0.7	**5.5**	2	0.7	**3.0**	2	0.0
H03[a]	**1.3**	2	0.4	**5.5**	2	0.7	**9.0**	2	1.4	**7.5**	2	2.1	**4.5**	2	0.7
H04	**6.8**	4	1.8	**9.0**	4	0.0	**12.5**	4	1.3	**7.5**	4	1.3	**4.3**	4	1.0
H08	**12.3**	3	2.4	**9.0**	3	0.0	**12.0**	3	1.7	**7.0**	3	1.7	**4.0**	3	1.0

[a]Sediments in some cores from H03 contained shell hash and were not included in analysis of the SPI data.

Table 3. Factor loading from PCA of water depth, bottom water temperature, and square root transformed and normalized sediment data. Variance explained for PC1, PC2, and PC3 is 42.8, 21.2, and 11.8%, respectively.

Variable	PC1	PC2	PC3
DIC	0.067	0.394	-0.072
Fe^{2+}	-0.022	0.267	0.238
$FeT_{(aq)}$	-0.074	0.305	0.232
$Mn_{(aq)}$	-0.307	0.006	-0.050
Water Depth	-0.199	-0.307	0.229
Temperature	0.145	0.220	-0.353
NH_4^+	0.070	0.397	-0.114
$Fe(II)_{HR}$	-0.13	0.338	-0.063
$Fe(T)_{NP}$	-0.308	-0.069	-0.055
$Fe(T)_{HR}$	-0.289	0.058	-0.095
$Fe(III)_{HR}$	-0.271	-0.061	-0.094
Mn(s)	-0.300	-0.015	-0.181
ON	-0.275	0.148	0.028
OC	-0.271	0.192	0.018
Inorganic C	0.166	-0.254	0.107
Porosity	-0.306	0.068	0.122
Density	-0.157	0.022	0.002
% Water	-0.306	0.055	0.096
Sulfate reduction	-0.14	-0.049	-0.412
py-Fe	-0.047	-0.088	-0.484
aRPD	-0.241	-0.222	0.222
D_B	0.052	0.250	0.380

EMS Table 2